INTERNATIONAL JOURNAL FOR NUMERICAL METHODS IN FLUIDS
Int. J. Numer. Meth. Fluids **30**: 795–811 (1999)

EFFICIENT SOLVING METHOD FOR UNSTEADY INCOMPRESSIBLE INTERFACIAL FLOW PROBLEMS

STÉPHANE VINCENT* AND JEAN-PAUL CALTAGIRONE

Modélisation Avancée des Systèmes Thermiques et Écoulements Réels (MASTER), Université de Bordeaux I, Avenue Pey-Berland, BP 108, 33402 Talence Cedex, France

SUMMARY

Unsteady interfacial problems, considered in an Eulerian form, are studied. The phenomena are modeled using the incompressible viscous Navier–Stokes equations to get the velocity field and an advection equation to predict interface evolutions. The momentum equation is solved by means of an implicit hybrid augmented Lagrangian–Projection method, whereas an explicit characteristic method coupled with a TVD SUPERBEE scheme is applied to the advection equation. The velocity components and the pressure are discretized on staggered grids with finite volumes. Emphasis is on the accuracy and robustness of the techniques described before. A precise explanation on the validation phase will be given, which uses such tests as the advection of a step function or Zalesak's problem to improve the calculation of the interface. The global approach is used on a physically hard interfacial test with strong disparities between viscosities and densities. Copyright © 1999 John Wiley & Sons, Ltd.

KEY WORDS: Navier–Stokes; incompressible; viscous; interfacial flow; augmented Lagrangian; projection method; TVD

1. INTRODUCTION

Even if formidable difficulties are encountered in both experimental and numerical work on 3D multi-phase flows, a large number of natural and technological processes imply the understanding of such problems [28]. Presented in this paper is a full numerical method, easy to implement in 3D, dedicated to multi-phase flows and able to solve strongly variable characteristic flows (viscosity and density ratios $> 10^4$).

In incompressible multi-phase flow problems, to estimate precisely free-surface evolutions, verifying the incompressibility constraint through the interface, with a nearly computer precision error, is primordial. To solve precisely the incompressible viscous Navier–Stokes equations, the projection method (see Goda [1]) is a good way of getting a velocity field verifying the constraint $\mathrm{div}(\vec{u}) = 0$, assuming an error of 10^{-13} (computing error). In our problem, the difficulty is due to the strong disparity of density and viscosity in the different fluids. Indeed, when we solve the Poisson equation, we need to do too many iterations to find the pressure under the constraint $\mathrm{div}(\vec{u}) = 0$. Another difficulty lies in the coupled Dirichlet–Neumann boundary conditions of our problem: in fact, the projection method is efficient when you only use Neumann boundary conditions. To speed the solving and to get pretty good

* Correspondence to: MASTER-ENSCPB, Université de Bordeaux I, Avenue Pey-Berland, BP 108, 33402 Talence Cedex, France.

CCC 0271–2091/99/140795–17$17.50

Received September 1997
Revised August 1998

estimations of the Neumann boundary conditions, we have coupled the projection method with an augmented Lagrangian method (see Fortin and Glowinsky [2]). The augmented Lagrangian solves the Navier–Stokes equations giving a velocity field verifying the constraint $\mathrm{div}(\vec{u}) = 0$ with a 10^{-5} precision. The velocity field is used as a valuator for the first step of the projection method. The Poisson equation is then solved. This way we have obtained a more accurate hybrid method, which is better than the augmented Lagrangian method, and performs better than the projection one.

Currently, there are two different ways of modeling interfacial flows. On the one hand, you can use adaptative grids in order to describe precisely the physical phenomena on the interface (surface tension, surface waves, etc.). In fact, this approach considers a Lagrangian or Lagrangian–Eulerian grid adapting its solving to the surface evolutions (see Magnaudet [3] and Floryan [4]). Magnaudet has obtained very good results studying bubble oscillations in 2D. However, this adaptative method becomes unusable as soon as the variations of the interface become significant. Indeed, it is very time-consuming to get a refined grid while preserving the good properties of orthogonality when the surface varies strongly. The use of such a method in 3D with strong surface evolutions is not realistic.

On the other hand, you can use a fixed staggered Cartesian grid (marker and cell (MAC)). In this case, the main problem results from finding an algorithm describing precisely the position of the interface. Different approaches exist to treat an interfacial flow on a Cartesian grid. The first one, called the 'marker method' (see Daly [5,6]) consists of putting markers on the interface at the initial time. Now you solve the Navier–Stokes equations and then, movement of the markers in the velocity field describes the evolution of the surface between the different fluids. To get the full interface, you have to build an interpolation between the markers, e.g. using a spline method. This algorithm gives accurate results in two dimensions with very simple programming. The marker technique contains, however, two principal drawbacks: there is no conservation of mass and the 3D extension remains too difficult because it is hard to determine a good spline surface interpolation in 3D.

Another commonly used approach to represent the interface with Cartesian grids is the volume of fluid (VOF) method (see Hirt-Nichols [7] and Zaleski [8]). On each defined volume-using cell centered on pressure, we consider a fractional function, called the color function $C_{i,j,k}$, corresponding to the volume of the fluid in cell (i, j, k). The process is made up of three steps. Knowing $C_{i,j,k}$, we build the interface as the surface discontinuity between the fluids. We next solve the Navier–Stokes equations to obtain the new velocity field. We finally move the interface at time n to obtain the new $C_{i,j,k}$ at time $(n+1)$. Youngs's VOF method (see Youngs [9]) provides very good results with a very satisfactory mass conservation. However, in the face of strong shears, if the interface is defined on a few cells, the VOF reconstruction brings about the appearance of scraps. Moreover, the computation requires a large investment that makes 3D use difficult. To finish with, we cannot use VOF schemes such as Youngs for more than two fluids.

To avoid the drawbacks of the marker and VOF methods, we choose to predict the interface evolutions by means of solving an advection equation. We define a color function $C_{i,j,k}$ equal to 1 in each cell filled with the lth fluid, $l = 0, p-1$ (p representing the number of fluids). The interfaces are represented by the discontinuities of $C_{i,j,k}$. If we have a velocity field, by solving an advection equation on the colour function we obtain the evolutions of the interfaces. The classic schemes do not offer good enough results: a first-order upwind scheme is too diffusive and a high-order scheme (Lax–Wendroff, Quick, ...) brings about oscillations due to the strong discontinuities between the different fluids. As a consequence, these types of schemes do not ensure a precise calculation of the interface. We have decided to apply the total variation

diminishing (TVD) theory (LeVeque [10], Yee [11,12] and Hirsch [13]) to the equation of $C_{i,j,k}$. The obtained scheme is of second-order, except near the discontinuities, where a first-order is enforced. The results set out on the following pages show the advantages of the TVD method: we get no oscillations, the diffusion is mainly controlled, the mass conservation is checked and the explicit computation is easy, even in 3D.

2. GOVERNING EQUATIONS

A 3D unsteady flow is modeled by means of the dimensional Navier–Stokes equations for incompressible fluids. In Cartesian co-ordinates, with a bounded domain Ω, we get

$$\nabla \cdot \vec{v} = 0, \tag{1}$$

$$\rho\left(\frac{\partial \vec{v}}{\partial t} + (\vec{v}\cdot\nabla)\vec{v}\right) = \rho\vec{g} - \nabla p + \nabla\cdot\left(\mu\left[\vec{\nabla}v + \left(\vec{\nabla}v\right)^T\right]\right), \tag{2}$$

where $\vec{v} = (u, v, w)^T$ is the velocity vector, p the pressure, ρ the density, μ the viscosity and g the gravity.

The different fluids are located by a color function $C_{i,j,k}$. In the presence of q fluids, we define $\Omega_l \subset \Omega$ as the domain containing the lth fluid $(0 \le l \le q-1)$. $\forall (x, y, z) \in \Omega_l$, we get

$$C(x, y, z) = l. \tag{3}$$

We define the interface between the fluids l and m $(0 \le l \le m \le q-1)$ as the average value of $C(x, y, z)$ for the values l and m. The surface evolutions are represented by an advection equation on C. $\forall (x, y, z) \in \Omega$, we obtain

$$\frac{\partial C}{\partial t} + \vec{v}\cdot\vec{\nabla}C = 0. \tag{4}$$

Since the viscosity μ and the density ρ of the mixed fluid are constant in each fluid, and knowing the position of the interfaces, we reorganize ρ and μ so as they take a different value according to the new arrangement of the fluids. Hence, we write

$$\text{if } C = l \text{ then } \begin{cases}\rho = \rho_l \\ \mu = \mu_l\end{cases}, \quad \text{else } C = \frac{l+m}{2} \quad \text{and} \quad \begin{cases}\rho = \dfrac{\rho_l + \rho_m}{2} \\ \mu = \dfrac{2\mu_l\mu_m}{\mu_l + \mu_m}\end{cases}, \tag{5}$$

where l and m indicate respectively, the lth and the mth fluids.

3. TVD SUPERBEE DISCRETIZATION FOR ADVECTION EQUATION

3.1. Description of the TVD SUPERBEE scheme

In this chapter, we present the treatment of the advection equation for the color function. The classical schemes (see Hirsch [13]) are not efficient enough: a first-order scheme, Upwind for example, is too diffusive [see Figure 1(a)]) and a high-order scheme, such as Lax–Wendroff, brings about oscillations [see Figure 1(b)]).

The results described by Figure 1 show how necessary it is to build a new scheme that is able to calculate precisely the interface. This remark is essential; indeed, the drawbacks observed in 1D will be developed in 2D or 3D. The solution follows from the following idea: as Equation (4) is hyperbolic, a good way of solving it is to apply the mathematical theory used in compressible fluid mechanics.

We define t as the time variable, V as the flow velocity and x as the 1D space variable. Hyperbolic problems are characterized by two fundamental properties: the signals are spreading with a finite velocity (property P1) and the representative quantities of the phenomenon (property P2) can contain discontinuities spreading or appearing during the evolutions. P1 involves the application of a characteristic method that demonstrates the conservation of the advection equation solutions on the $x - Vt = \text{constant}$ lines. Obtaining an initial condition, we know how to get the necessary information to calculate correctly the solution at time n. The property P2 requires the use of a robust scheme that is able to be applied in the presence of discontinuities. We also want a high-order scheme giving precise solutions. Such schemes come from the total variation diminishing (TVD) theory (see LeVeque [10]). A TVD scheme is characterized by the two following properties: in regular areas of the solution, the scheme is of high-order, and near the four discontinuities, it becomes of first-order. This construction obtains a non-oscillating scheme of high-order nearly in the whole solving domain. The non-oscillating property is obtained by limiting the conservative flux of a high-order scheme so as to check the TVD requirements, i.e.

$$\left(\frac{\sum_i \left| C_i^{n+1} - C_{i-1}^{n+1} \right|}{\Delta x} \leq \frac{\sum_i \left| C_i^n - C_{i-1}^n \right|}{\Delta x} \right).$$

We will now explain the way to build a TVD scheme of high-order. The 1D Lax–Wendroff discretization of Equation (4) by a characteristic method in a finite volume approximation is presented.

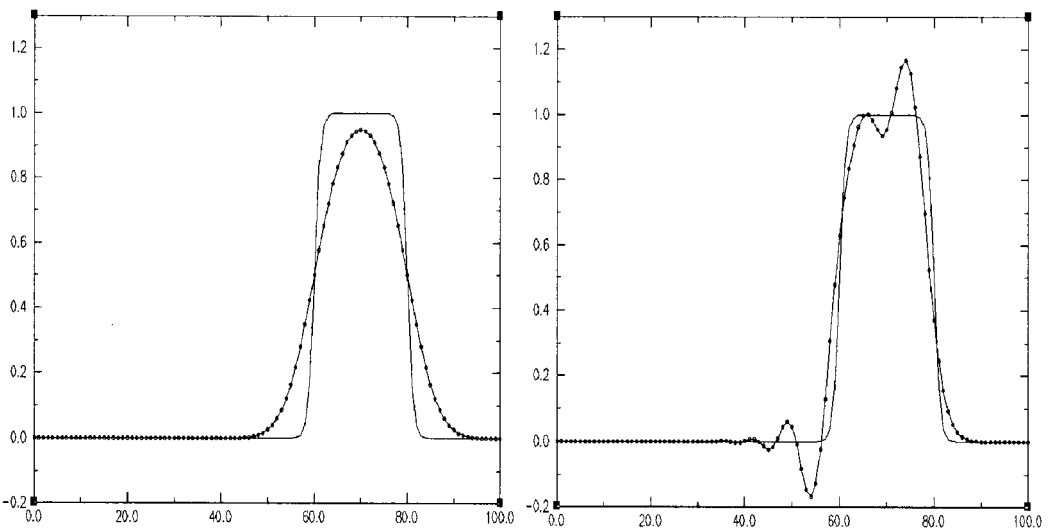

Figure 1. Simulation in 1D of the propagation at the step function $C(x) = (0.5 + 0.5 \tanh(80(x - 0.1)))$ on a 100 mesh grid (horizontal axis). Initially, $0 \leq C(x) \leq 1$ (vertical axis). Comparison after 100 iterations between an Upwind (a), a Lax–Wendroff (b) scheme and the analytical solution.

- Knowing the solution C_i^n of average values on the cells, we reconstruct it by a linear function on each cell. If γ_i^n is the slope of the linear reconstruction, then

$$\forall x \in [x_{i-1/2}, x_{i+1/2}], \quad \tilde{C}^n(t_n, .) = C_i^n + \gamma_i^n (x - x_i). \tag{6}$$

- Using the characteristic method, we exactly solve the advection equation for $\tilde{C}^n(t_n, .)$ between the times t_n and t_{n+1}. If Δx is the space scale and Δt the time scale, we get

$$\tilde{C}^n(t_{n+1}, .) = \tilde{C}(t_n, x - V\Delta t). \tag{7}$$

- We obtain C_i^{n+1} as the average of $\tilde{C}^n(t_{n+1}, .)$ on cell $[x_{i-1/2}, x_{i+1/2}]$:

$$\Delta x C_i^{n+1} = \int_{x_{i-1/2}}^{x_{i+1/2}} \tilde{C}^n(t_{n+1}, x)\, \mathrm{d}x.$$

Applying the characteristic method (7) with $V \geq 0$, we obtain

$$\Delta x C_i^{n+1} = \int_{x_{i-1/2}}^{x_{i+1/2}} \tilde{C}^n(t_n, x - V\Delta t)\, \mathrm{d}x = \int_{x_{i-1/2} - V\Delta t}^{x_{i+1,2} - V\Delta t} \tilde{C}^n(t_n, x)\, \mathrm{d}x.$$

Using the linear reconstruction (6), the solution becomes

$$\begin{aligned} \Delta x C_i^{n+1} &= \int_{x_{i-1/2} - V\Delta t}^{x_{i-1/2}} \tilde{C}_{i-1}^n + \gamma_{i-1}^n (x - x_{i-1})\, \mathrm{d}x + \int_{x_{i-1/2}}^{x_{i+1,2} - V\Delta t} \tilde{C}_i^n + \gamma_i^n (x - x_i)\, \mathrm{d}x \\ &= V\Delta t C_{i-1}^n + \frac{1}{2} V \gamma_{i-1}^n \Delta x \Delta t (1 - V\sigma) + (\Delta x - V\Delta t) C_i^n + \frac{1}{2} V \gamma_i^n \Delta x \Delta t (V\sigma - 1), \end{aligned}$$

where $\sigma = \Delta t / \Delta x$ is the CFL number.

We finally get the expression of C at time $n+1$:

$$C_i^{n+1} = C_i^n - V\sigma (C_i^n - C_{i-1}^n) + \frac{1}{2} V\sigma \Delta x (V\sigma - 1)(\gamma_i^n - \gamma_{i-1}^n). \tag{8}$$

Now, we have to choose a slope γ_i^n and the advection equation is completely discretized by expression (8). $\gamma_i^{n,\mathrm{LW}} = C_{i+1}^n - C_i^n / \Delta x$ corresponds to the Lax–Wendroff slope. This slope is chosen as a reference because of the good properties of the Lax–Wendroff scheme in the regular zones of the solution. We now study how to render TVD to the high-order oscillating Lax–Wendroff scheme chosen, to bring it robust properties near the discontinuities. It is possible to demonstrate that, in the three-step construction scheme (8), the solving and the projection steps are TVD. As a consequence, in the reconstruction step, only the slope choice can determine the TVD character of this scheme. Observing Figure 2(a), we can see that the Lax–Wendroff slope brings about extrema near the minima or the maxima of the average cell solution. In this case, we notice that the total variation is increasing: the Lax–Wendroff scheme is not TVD. The idea is to limit the slope $\gamma_i^{n,\mathrm{LW}} = (C_{i+1}^n - C_i^n)/\Delta x$, enforcing the condition $C_{i \mp 1/2}^{\mp} \in [C_{i-1}, C_i]$, where $C_{i-1/2}^-$ is the value for $x_{i-1/2}$ of the linear cell function in $[x_{i-3/2}, x_{i-1/2}]$ and $C_{i-1/2}^+$ is the value for $x_{i-1/2}$ of the linear cell function in $[x_{i-1/2}, x_{i+1/2}]$. Let us consider $\theta_i^n = (C_i^n - C_{i-1}^n)/(C_{i+1}^n - C_i^n)$, the new limited slope obtained is expressed as (see Hirch [13] and Sweby [14])

$$\gamma_i^{n,T} = \max(0, \min(1, 2\theta_i^n), \min(2, \theta_i^n)) \frac{C_{i+1}^n - C_i^n}{\Delta x} = \phi(\theta_i^n) \gamma_i^{n,LW}. \tag{9}$$

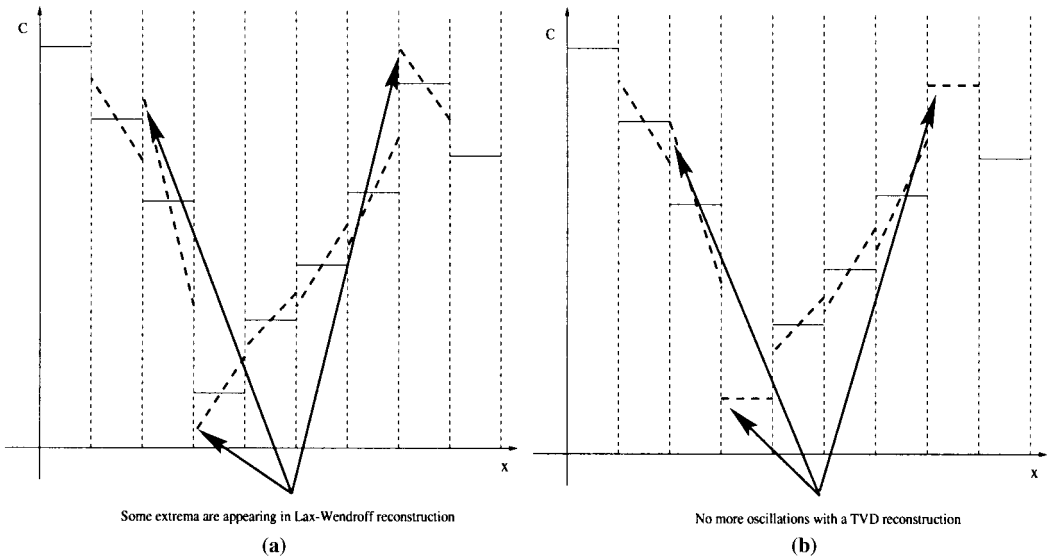

Figure 2. Example of 1D space reconstructions (horizontal axis) of C (vertical axis) in the case of a Lax–Wendroff scheme (a) and of a TVD SUPERBEE scheme (b).

In fact, $\phi(\theta_i^n)$ is a correcting flux equal to 1 in the whole solving domain, except near the extrema where this flux limits the Lax–Wendroff slope. The results obtained with $\gamma_i^{n,T}$ (see Figure 2(b)) show that the TVD properties are respected.

The TVD scheme built above is called the Lax–Wendroff TVD SUPERBEE scheme. The final expression in 1D for any V is:

$$C_i^{n+1} = C_i^n - \sigma \max(0, V)(C_i^n - C_{i-1}^n) + \frac{1}{2}\sigma\Delta x \max(0, V)(V\sigma - 1)(\phi_i^n \gamma_i^{n,\mathrm{LW}} - \phi_{i-1}^n \gamma_{i-1}^{n,\mathrm{LW}})$$
$$- \sigma \min(0, V)(C_{i+1}^n - C_i^n) + \frac{1}{2}\sigma\Delta x \min(0, V)(V\sigma + 1)(\phi_{i+1}^n \gamma_{i+1}^{n,\mathrm{LW}} - \phi_i^n \gamma_i^{n,\mathrm{LW}}). \tag{10}$$

Figure 3 shows the results obtained with the scheme (10) for the same case as in Figure 1. The solution is nearly equal to the analytical solution. We have corrected the drawbacks of the Upwind (diffusion) and Lax–Wendroff (oscillations) schemes.

We will now present some applications that will allow us to judge the performance of our TVD scheme (10) in 2D and 3D. The 2D or 3D form of (10) is immediately deduced from a transposition of the x-direction flux to y- and z-directions. If you solve the three directions at the same time, some distortions appear in the diagonal directions. As a consequence, we have cut the time scale into three parts [27]. In each part, we solve one direction. Considering V_x, V_y and V_z as the velocities in each direction, the 3D explicit splitting Lax–Wendroff TVD SUPERBEE scheme so obtained is

$$C_{i,j,k}^{n+1/3} = C_{i,j,k}^n - \sigma \max(0, V_x)(C_{i,j,k}^n - C_{i-1,j,k}^n)$$
$$+ \frac{\sigma}{2}\Delta x \max(0, V_x)(V_x\sigma - 1)(\gamma_{i,j,k}^{n,T} - \gamma_{i-1,j,k}^{n,T}) - \sigma \min(0, V_x)(C_{i+1,j,k}^n - C_{i,j,k}^n)$$
$$+ \frac{\sigma}{2}\Delta x \min(0, V_x)(V_x\sigma + 1)(\gamma_{i+1,j,k}^{n,T} - \gamma_{i,j,k}^{n,T}),$$

$$C_{i,j,k}^{n+2/3} = C_{i,j,k}^{n+1/3} - \sigma \max(0, V_y)(C_{i,j,k}^{n+1/3} - C_{i-1,j,k}^{n+1/3}) + \frac{\sigma}{2}\Delta y \max(0, V_y)(V_y\sigma - 1)(\gamma_{i,j,k}^{n+1/3,T} - \gamma_{i-1,j,k}^{n+1/3,T}) - \sigma \min(0, V_y)(C_{i,j+1,k}^{n+1/3} - C_{i,j,k}^{n+1/3}) + \frac{\sigma}{2}\Delta y \min(0, V_y)(V_y\sigma + 1)(\gamma_{i,j+1,k}^{n+1/3,T} - \gamma_{i,j,k}^{n+1/3,T}), \tag{11}$$

$$C_{i,j,k}^{n+1} = C_{i,j,k}^{n+2/3} - \sigma \max(0, V_z)(C_{i,j,k}^{n+2/3} - C_{i,j,k-1}^{n+2/3}) + \frac{\sigma}{2}\Delta z \max(0, V_z)(V_z\sigma - 1)(\gamma_{i,j,k}^{n+2/3,T} - \gamma_{i,j,k-1}^{n+2/3,T}) - \sigma \min(0, V_z)(C_{i,j,k+1}^{n+2/3} - C_{i,j,k}^{n+2/3}) + \frac{\sigma}{2}\Delta z \min(0, V_z)(V_z\sigma + 1)(\gamma_{i,j,k+1}^{n+2/3,T} - \gamma_{i,j,k}^{n+2/3,T}).$$

3.2. Validation on simple two-fluid advection tests

In this section, the advection of C is not coupled to the solutions of the momentum equations. Simple advection tests on analytical velocity fields are proposed.

• To begin with, we study the advection in 2D of a 0.15 m radius circle in a constantly turning velocity field. This test is important because it does not favor any directions. It is a good way of checking the validity of the scheme. We choose a time scale $\Delta t = 0.001$ s on an 80×80 grid. The domain Ω is Ω is 1 m^2. $\forall (x, y) \in \Omega$, the velocity field $\vec{u}(x, y) = (U(x, y), V(x, y))$ is described by

$$U(x, y) = -\frac{\pi}{2}\left(y - \frac{L}{2}\right) \quad \text{and} \quad V(x, y) = \frac{\pi}{2}\left(x - \frac{L}{2}\right). \tag{12}$$

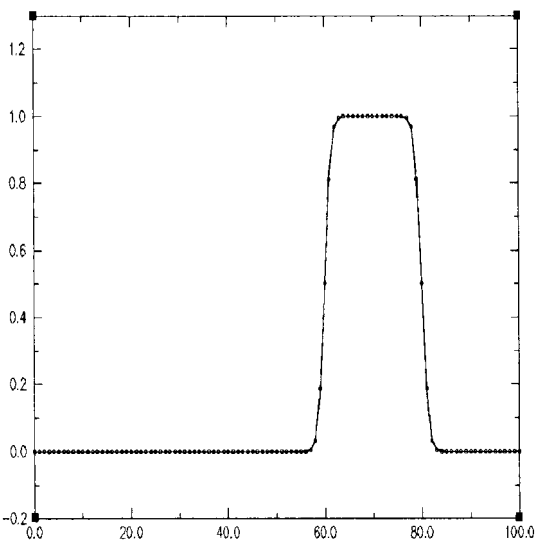

Figure 3. Simulation in 1D of the propagation of the step function $(0.5 + 0.5 \tanh(80(x - 0.1)))$. Comparison after 100 iterations between the Lax–Wendroff TVD SUPERBEE scheme and the analytical solution.

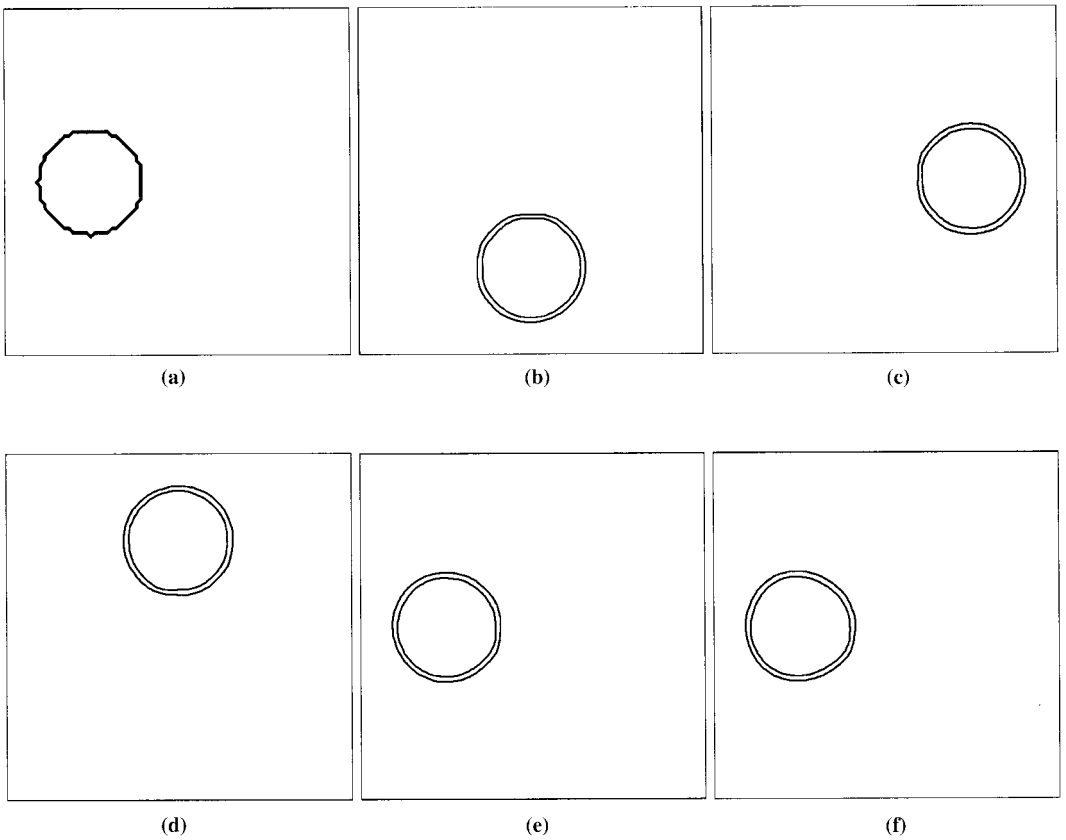

Figure 4. Advection of a circle in a turning velocity field—the figures present the initial condition on a 80×80 grid (a) and the results after 500 (b), 1000 (c), 1500 (d), 2000 (e) and 20000 (f) iterations. (Visualization of the iso-values 0.01 and 0.99 of C.)

The results obtained (Figure 4) are spreading with good velocity and with a 10^{-5} mass conservation error, which is quite satisfactory. After one turn (2000 iterations), the geometry of the circle is pretty good with respect to the initial condition. Even after ten turns, the simulation still has a good performance, even if a small deformation appears (due to the constraints of the Cartesian grid). We notice that the diffusion of the explicit splitting TVD SUPERBEE Lax–Wendroff scheme (11) is fixed during the calculations (two cells), which appears very interesting.

- The second application we decided to set out is Zalesak's problem: a slotted circle rotates in a constant turning velocity field (12). As explained by Rudman [15], this test is considered a difficult simulation for scalar advection methods. Indeed, near the sharp corners there are not enough cells to resolve the advection equation correctly with our TVD scheme. We present the calculations after one turn on a 150×150 grid with $\Delta t = 0.002$ s. The diameter of the circle is 0.8 m and the domain is 1 m^2.

The results obtained (see Figure 5) are in good agreement with the exact solution with a mass conservation error equal to 10^{-5}. Even if a Eulerian numerical scheme cannot resolve perfectly the singularity at the sharp corners moving in a turning velocity field, the problem is solved well through the TVD scheme that maintains a consistent interface shape. The diffusion

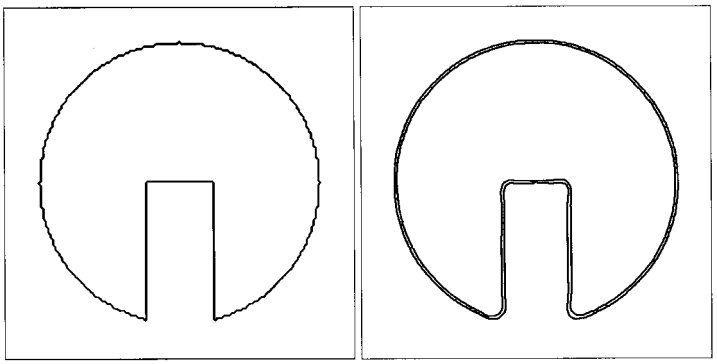

Figure 5. Simulation of Zalesak's problem on a 150×150 grid—description of the initial condition (a) and of the result after one turn (approximately 5000 iterations (b). (Visualization of the iso-values 0.01 and 0.99 of C.)

is concentrated on two cells and stays on two cells during the calculations, which corresponds to the good property observed in the previous test.

• The third test consists in translating a 0.2 m side square. Two velocity fields are considered: the first one is aligned with the co-ordinate axes, whereas the second one forms an angle of 45° with the axis. The velocity magnitude is equal to 1 m s^{-1} in both cases. The simulation is done on a 100×100 grid with $\Delta t = 0.001$ s. The domain is 1 m^2.

We can easily check that the translation is perfectly calculated through the TVD scheme, with a 10^{-5} mass conservation error, similar to the previous tests. Moreover, the diffusion is not dependent on the x- or y-axis, and stays on two cells during the solving iterations without growing (see Figures 6(b) and 7(b)).

In Section 4, to avoid the distortions due to the Cartesian grid, we have chosen to split one solving time step into several parts, each part resolving the problem in 1D (x, y or z). The results coming from the previous choice are very good and no distortions appear in the oblique translation (see Figure 7(b)).

• The first three tests we have presented have shown the very good properties of the TVD scheme for interfaces moving without deformations. To get a complete description of the phenomena dealing with interfacial flows, we have to study the case of topological change in the solution. It is very important to have the possibility of calculating the interface in the

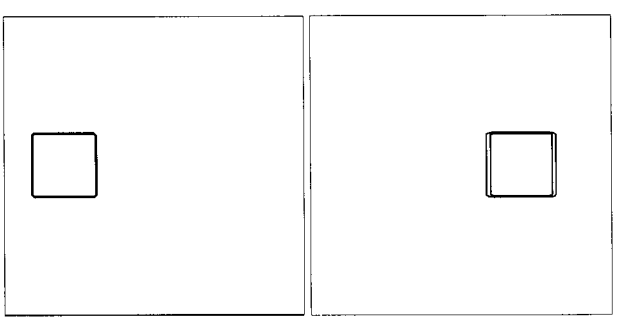

Figure 6. Translation of a square in an horizontal velocity field with a 100×100 grid—description of the initial condition (a) and of the result after 500 iterations (b). (Visualization of the iso-values 0.01 and 0.99 of C.)

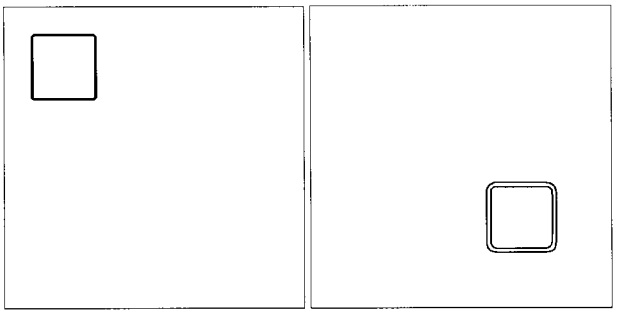

Figure 7. Translation of a square in an oblique velocity field with a 100×100 grid—description of the initial condition (a) and of the result after 500 iterations (b). (Visualization of the iso-values 0.01 and 0.99 of C.)

presence of shearing flows because they are often found in physical experiments. The simulation consists in deforming a circle in a shearing velocity field. We choose a 150×150 grid on a 1 m long square domain, with $\Delta t = 0.001$ s. If $(x, y) \in [0, 1] \times [0, 1]$ is a point in the square domain and $(x_0, y_0) \in [0, 1] \times [0, 1]$ are the co-ordinates of the domain center, the velocity field $\vec{u}(x, y) = (U(x, y), V(x, y))$ is defined as

$$U(x, y) = K \cos(\pi(x - x_0)) \sin(\pi(y - y_0)) \quad \text{and}$$
$$V(x, y) = -K \sin(\pi(x - x_0)) \cos(\pi(y - y_0)), \tag{13}$$

where K is a fraction constant of π.

In this case, the initial circle is deformed (see Figure 8(b) and (c)) during N iterations; we reverse the sign of the shearing velocity field (17) and we perform N iterations more (see Figure 8(e) and (f)). After N steps forward followed by N steps backward, a perfect solving would give the initial condition. With $N = 1000$ (see Figure 8(b) and (e)), we get a very satisfying solution: indeed, the diffusion due to the distortion (Figure 8(b)) does not damage the final result (Figure 8(f)), which fits well the initial solution (the solution with $N = 1000$ is almost as good as in translation or rotation tests). If we take $N = 4000$ (see Figure 8(c) and (f)), the results are less precise. In fact, the stretching out zones of the interface, coming from the strong distortions, do not give enough solving points to the TVD SUPERBEE scheme. In these zones, the TVD SUPERBEE scheme detects almost all extrema in the color function. Consequently, it is always of first-order and therefore diffusive (see Figure 8(c)). The solution after 4000 steps backward is physically coherent but some diffusion and some distortions have appeared. They are the direct consequence of the difficulties described before.

- To finish with, we test a 3D advection: a sphere is submitted to a rotation velocity field. If Ω is a cubic domain, $\forall (x, y, z) \in \Omega$, the velocity field is described by the three components of $\vec{u}(x, y, z) = (U(x, y, z), V(x, y, z), W(x, y, z))$:

$$U(x, y) = -\frac{\pi}{2}\left(y - \frac{L}{2}\right), \qquad V(x, y) = \frac{\pi}{2}\left(x - \frac{L}{2}\right) \quad \text{and} \quad W(x, y) = 0. \tag{14}$$

The test consists of advecting a sphere in a turning roller velocity. Ω is a 1 m side cubic domain. We choose a $32 \times 32 \times 32$ grid with $\Delta t = 0.01$ s. The results obtained (see Figure 9(a)–(f)) are very interesting because the TVD SUPERBEE scheme provides results in 3D with the same good properties as in 2D, without any programming work. The sphere is advected correctly with a 10^{-4} mass conservation error. If we look to a $z = 0.5$ m plane cut (see Figure

9(g)–(i)), we discover that the diffusive zones at the interface after one turn (see Figure 9(e)) and after five turns (see Figure 9(f)) are not more important than in 2D (see Figure 4). In fact, the diffusion stays on two cells during the calculations in 2D and in 3D.

After one turn (Figure 9(e)) and after five turns (Figure 9(f)), the morphology of the sphere remains correct, without any distortions: we can say that the splitting scheme in 3D is as efficient as the one in 2D. Figure 9(g)–(i) show that some deformations of the sphere appear during the calculations. This phenomenon is principally due to the weak precision of the grid, which makes the initial condition not very precise. To get better results, it will be sensible to take a refined grid ($80 \times 80 \times 80$, for example). Then we could expect to get a precise solution with a good interface definition.

4. HYBRID SOLVING METHOD FOR NAVIER–STOKES EQUATIONS

We will now set out the method we have used to solve numerically the incompressible viscous Navier–Stokes equations (1) and (2). In our simulations, an augmented Lagrangian or a

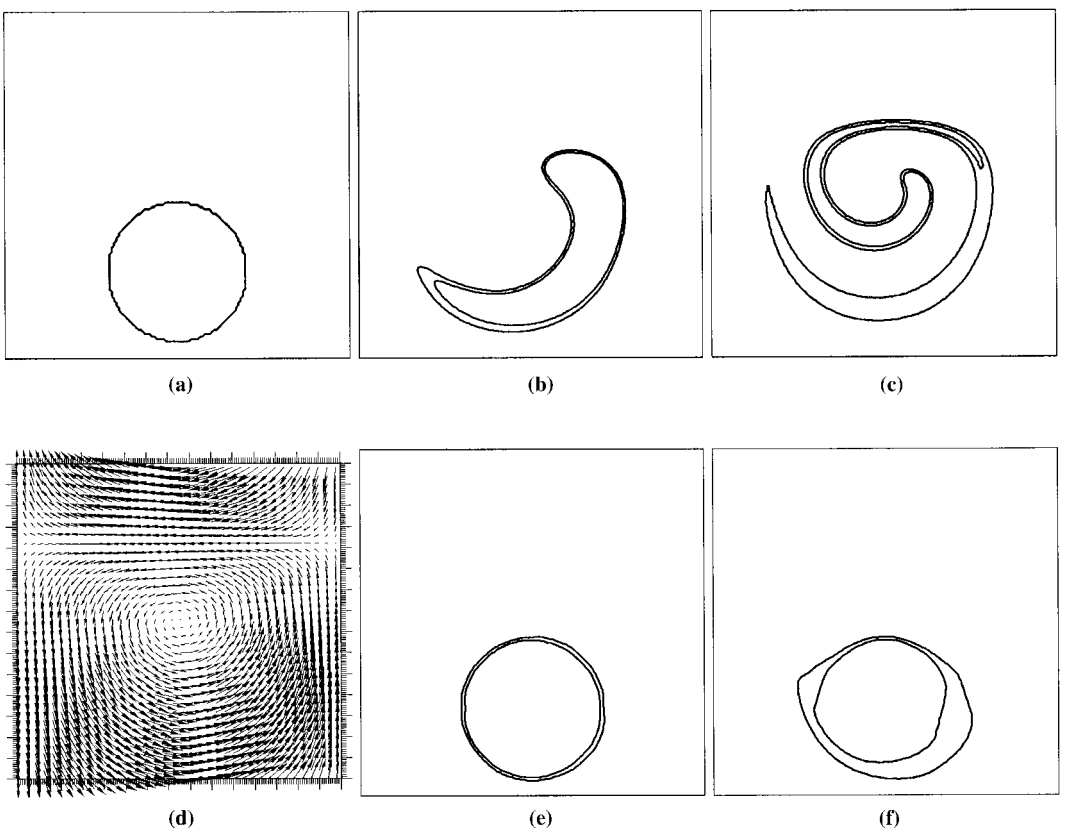

Figure 8. Advection of a circle in a shearing velocity field on a 150×150 grid: (a) presents the initial condition, (d) is the velocity field, (b) and (e) show the results of the calculations after 1000 iterations with the velocity field (13) and 1000 iterations more with a reverse sign in (13), and (c) and (f) describe the solution after 4000 iterations with the velocity field (13) and 4000 iterations more with a reverse sign in (13). (Visualization of the iso-values 0.01 and 0.99 of C.)

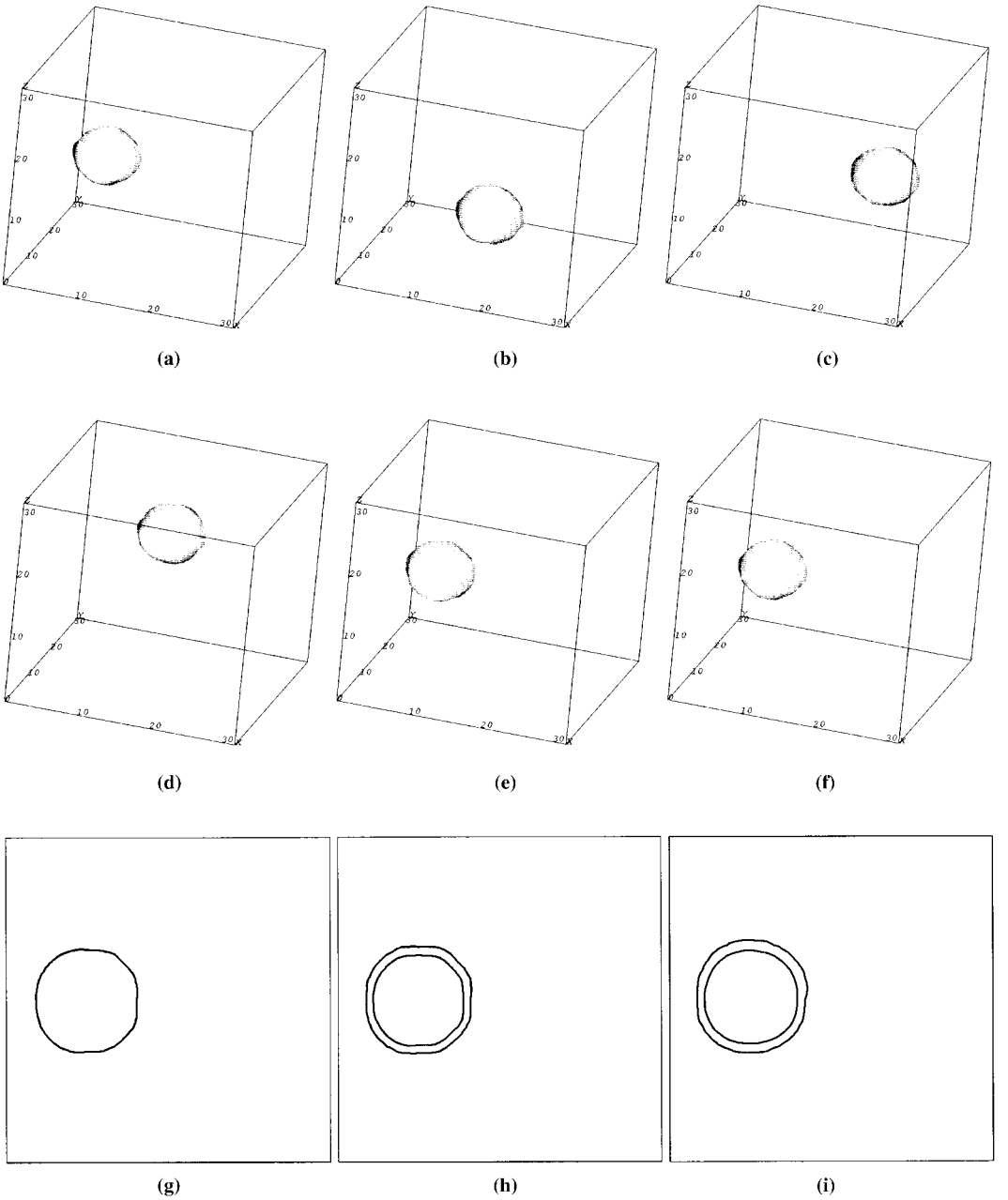

Figure 9. Advection of a sphere in a turning velocity field on a $32 \times 32 \times 32$ grid (a) presents the initial condition in 3D, (b)–(f) show the results of the calculations in 3D after 100, 200, 300, 400 and 2000 iterations respectively, (g–(i) describe a cut in the $z = 0.5$ m plan for the initial condition and the solution after 400 and 2000 iterations. (Visualization of the iso-value 0.5 of C from (a) to (f) followed by the 0.01 and 0.99 one from (g) to (i).)

projection method are not efficient because of the strong density and viscosity gradients near the interface. The augmented Lagrangian (see Fortin and Glowinsky [2] and Nicolas [16]) solves the Navier–Stokes equations correctly in each of the fluids (the mass balance is

verified), but near the interface, Equation (2) is not calculated with sufficient precision and there is no continuity on the velocities. Concerning the projection method (see Goda [1]), the method requires a lot of iterations to solve the Poisson equation and get a velocity field verifying $\mathrm{div}(u) = 0$, with a 10^{-13} error. Moreover, the presence of Dirichlet boundary conditions in our problems destabilizes the projection solving, which is well-formulated for Neumann boundary conditions (Peyret and Taylor [17]).

To improve the projection method, we choose to use the augmented Lagrangian as a valuator of the auxiliary velocity and pressure in the first step of the projection method. As a consequence, we obtain the unknowns correctly estimated at the boundary conditions and in the fluids. The second step, in which we solve a Poisson equation, allows us to get a very good mass balance, even near the interface: the Poisson equation acts as a smoothing operator on the new velocity field calculated in a third step.

Considering Euler schemes of first-order on the time operators and taking an auxiliary velocity U^* and a corrective pressure P^*, the hybrid method is written as:

- (I) A predictive step with the augmented Lagrangian

$$p^{n+1/2} = p^n - s\nabla\cdot U^{*,n+1}. \tag{15}$$

The pressure (6) estimated at $(n+1)\Delta t$ is expressed in the momentum equation.

$$\frac{\partial U^*}{\partial t} + U^n\cdot\nabla U^{*,n+1} - \frac{r}{\rho}\nabla(\nabla\cdot U^{*,n+1}) = -\frac{1}{\rho}\nabla p^n + g - \frac{1}{\rho}\nabla\cdot[\mu(\nabla U^{*,n+1} + \nabla^t U^{*,n+1})]. \tag{16}$$

We define $P^{*,n}$ as $p^{n+1/2}$.

- (II) A projection step with the Poisson equation

$$\nabla\cdot\left(\frac{\nabla p^*}{\rho}\right) = -\nabla\cdot U^{*,n+1}, \quad \frac{\partial p^*}{\partial n} = 0. \tag{17}$$

- (III) An evaluation step at time $(n+1)\Delta t$

$$U^{n+1} = \left(U^{*,n+1} - \frac{\Delta t}{\rho}\nabla p^{*,n+1}\right), \quad p^{n+1} = p^{*,n} + p^{*,n+1}. \tag{18}$$

The parameters s and r control the numerical treatment of incompressibility. The algorithm (15)–(18) allows us to solve the Navier–Stokes equations with different methods: taking $r = 0$ and $s = r$, we get the projection method, taking $0 < r \ll 1$ and $s = r$, we obtain the hybrid solving method, and taking r of first-order (switching steps (II) and (III)) and $s = r$, we use the augmented Lagrangian method. We can even solve the problem by means of an Uzawa algorithm, taking $r = 0$ and $0 < s \ll 1$, switching steps (II) and (III).

The hybrid method permits the use of both Neumann and Dirichlet boundary conditions. In the first step of the hybrid method, we choose an iterative BICGSTAB solver (biconjugate stabilized gradient) with a preconditioning based on a modified and incomplete Gauss factorization MILU (see Van Der Vorst [18] and Gustafssons [19]) to calculate the Navier–Stokes equations by an implicit augmented Lagrangian. The hybrid method has been validated in different simulations (natural convection [20], flows around a cylinder, . . .).

5. SIMULATION OF VISCOUS TWO-FLUID INTERFACIAL PROBLEMS WITH THE COUPLED HYBRID/TVD SUPERBEE METHOD

The study proposed in this section presents two main interests: firstly, the strong viscosity and density gradients represent a physically hard problem for the method described above, and moreover, the research in numerical solving methods for difficult interfacial problems corresponds to an important industrial request. The experiment corresponds to a Newtonian jet filling a square box, open in its upper part. Initially, the cavity is full of air. We wish to study the evolution of the jet morphology in accordance with the velocity inlet and the box dimensions.

The characteristics of the simulations are as follows:

Liquid
Viscosity $= 300$–600 Pa s
Density $= 1800$ kg m^{-3}
Air
Viscosity $= 1.85 \times 10^{-5}$ Pa s
Density $= 1.1768$ kg m^{-3}

Experiment 1:

Square cavity of size 1×1 m^2
Inlet velocity equal to 1 m s^{-1} and inlet width equal to 0.12 m
Liquid viscosity equal to 300 Pa s
$Re = 0.72$
$H/D = 8.33$

Experiment 2:

Square cavity of size 1×1 m^2
Same inlet velocity, and inlet width equal to 0.1 m
Liquid viscosity equal to 500 Pa s
$Re = 0.36$
$H/D = 10$

If we refer to the article of Tomé *et al.* [21], we get a physical criterion that establishes the experiments with buckling jets. This criterion is based on experimental and approximate theoretical results. It has been argued that for a planar jet (2D), buckling will occur if the following restrictions are satisfied:

$$Re < 0.56$$

and

$$\frac{H}{D} > 3\pi, \tag{19}$$

where Re is the Reynolds number based on the slit width D, and H is the height of the inlet above the bottom of the cavity.

A comparison with (19) shows that experiment 1 does not correspond to a buckling jet, whereas experiment 2 does. We will discover next that the simulations are in agreement with

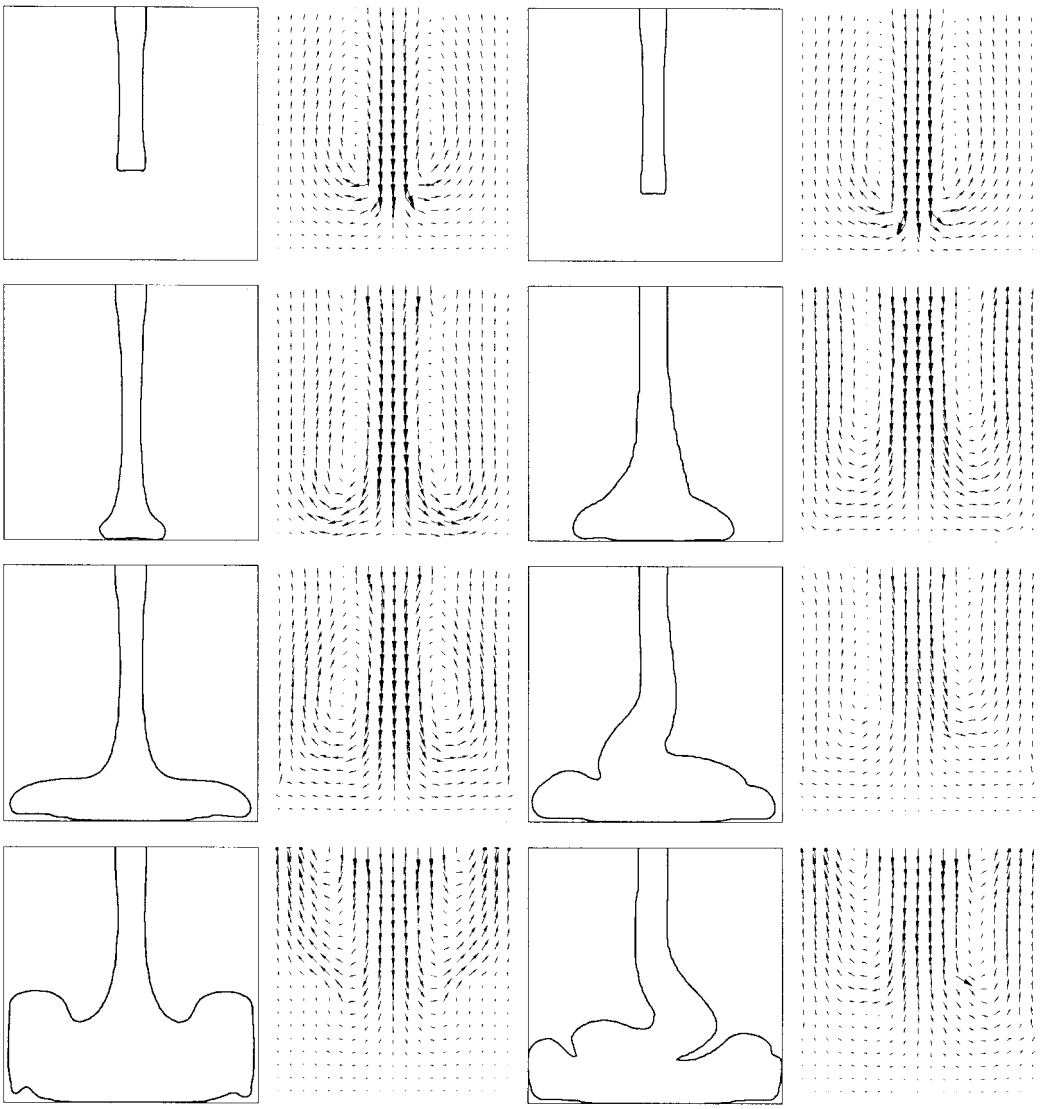

Figure 10. Simulation of a jet injected in a square cavity on a 80×80 grid—the columns (a) (the interface) and (b) (the velocity field) present the results after 400, 600, 1400 and 2800 iterations for a 1 m s^{-1} velocity imposed on the inlet with a 1 m square cavity and the columns (c) (the interface) and (d) (the velocity field) describe the solution after 500, 1500, 2200 and 2600 iterations for a 1 m s^{-1} velocity imposed on the inlet with a 1 m square cavity. (Visualization of the iso-value 0.5 of C.)

the theoretical criterion (19). Indeed, Figure 10(a) and (b) (experiment 1) show a jet flowing laterally and filling the cavity. As expected in (19), there is no buckling. Now, if we observe the simulation results corresponding to experiment 2 (Figure 10(c) and (d)), we get a buckling jet going from right to left alternatively. In this case, the Newtonian fluid accumulates, obstructs the oncoming fluid and leads to buckling. The striction phenomenon is well-retranscribed in both experiments, which means that we correctly anticipate the viscous and the gravity effects.

The numerical calculations with the hybrid method provide a very good velocity field (Figure 10(b) and (d)). The velocities in the inlet jet must become almost zero near the bottom part of the cavity. We can also see the ejection of air by the opened upper part of the cavity. Concerning the interfacial treatment, the results are quite satisfying. Indeed, on a reasonable grid (80×80), the explicit TVD method gives a good description of the interface by means of the 0.5 iso-value of the color function. We have not met with particular problems due to the numerical treatment of the interface, except perhaps with the weak diffusion appearing during the calculations (as explained in Section 4). To finish with, we can say that the symmetry of the numerical flow solutions, observed in the first experiment, testifies to the good solving of the problem with the coupled hybrid/TVD method.

6. CONCLUSION AND DISCUSSION

In this paper, we have proposed a hybrid solving method for the Navier–Stokes equations that has demonstrated its very efficient behavior when solving difficult unsteady incompressible interfacial flows. This point is very important because it conditions the solving of the interfacial evolutions: indeed, the surface between two or more fluids moves in conjunction with the velocity field due to the solving of Navier–Stokes equations.

The second approach detailed in this article was the solving of an advection equation on a color function to describe the evolutions of the interfaces. The explicit splitting TVD SUPERBEE method chosen has shown very interesting results with a weak mass conservation error, no oscillations due to the discontinuities appearing near the interface, with a controlled diffusion and an easy explicit computation. The scheme has been fully validated in 1D, 2D and 3D. The performance on the physical simulation has proved how interesting it is in the presence of strong stretching out zones, particularly for the future 3D tests.

The calculation of a 3D jet will be the next work to be done: this is one of the main motivations of this study. The results obtained in the validations make us optimistic with regard to the good behavior of the coupled hybrid/splitting TVD SUPERBEE method in 3D. Another physical context that has to be developed is multiphase flow problems (with the 3D context, it is our other strong motivation). Indeed, these problems are easy to define with a color function, as explained in Section 2. If there is N fluids, the advection equation solves the color function evolutions in presence of N fronts. To finish with, it will be interesting to treat the surface tension in case our jet problem is about a weak velocity inlet. To do so, a tensor term is added in the momentum conservation equation acting as a volume force on the free surface (Brackbill [22]). We have validated the coupled hybrid/TVD method with the surface tension treatment on experimental measurements (Martin and Moyce [23]). Qualitative and quantitative comparisons show good agreements between experimental and numerical results.

Some numerical improvement will be probably done using ENO schemes instead of the TVD SUPERBEE method (see Wang and Osher [24] and Perrel [26]). Indeed, the diffusion appearing in the strong stretching out zone will be reduced with these new schemes. The adaptation of a level set method to our problem (if it is possible to think of the 3D context

with multiphasic flows) would certainly be the best solution to define precisely the evolutions of the interfaces (see Sussman and Smereka [25]).

REFERENCES

1. K. Goda, 'A multistep technique with implicit difference schemes for calculating two- or three-dimensional cavity flows', *J. Comput. Phys.*, **30**, 76–95 (1978).
2. M. Fortin and R. Glowinsky, 'Methodes de Lagrangien augmenté. Application à la résolution numérique de problèmes aux limites', *Dunod*, 1982.
3. J. Magnaudet, M. Rivero and J. Fabre, 'Accelerated flows around a rigid sphere or a spherical bubble', *J. Fluid Mech.*, **284**, 97–136 (1995).
4. J.M. Floryan and H. Rasmussen, 'Numerical methods for viscous flows with moving boundaries', *Appl. Mech. Rev.*, **42**, 323–340 (1989).
5. B.J. Daly, 'Numerical study of two-fluid Rayleigh–Taylor instability', *Phys. Fluids*, **10**, 297–307 (1967).
6. B.J. Daly, 'Numerical study of the effect of surface tension on interface instability', *Phys. Fluids*, **12**, 1340–1354 (1969).
7. C.W. Hirt and B.D. Nichols, 'Volume of fluid (VOF) methods for the dynamics of free boundaries', *J. Comput. Phys.*, **39**, 201–255 (1981).
8. S. Zaleski, J. Li, R. Scardovelli and G. Zanetti, 'Direct simulation of multiphase flows with density variations', in Colloque IUTAM *Variable Density Low Speed Turbulent Flows*, Kluwer, Dordrecht, 1996.
9. D.L. Youngs, 'Time-dependent multimaterial flow with large fluid distortion', in K.W. Morton and M.J. Baines (eds.), *Numerical Methods for Fluid Dynamics*, Academic, New York, 1982, pp. 273–285.
10. R.J. LeVeque, 'Numerical methods for conservation laws', in *Lecture in Mathematics*, Birkhauser, Zurich, 1990.
11. N.D. Sandham and H.C. Yee, 'A numerical study of a class of TVD schemes for compressible mixing layers', NASA, 1989.
12. H.C. Yee, 'Upwind and symmetric shock capturing schemes', NASA, 1987.
13. C. Hirsch, *Numerical Computation of Internal and External Flows*, Wiley, New York, 1990.
14. P.K. Sweby, 'High resolution schemes using flux limiters for hyperbolic conservation laws', *SIAM J. Numer. Anal.*, **21**, 995–1011 (1984).
15. M. Rudman, 'Volume tracking methods for interfacial flow calculations', *Int. J. Numer. Methods Fluids*, **24**, 671–691 (1997).
16. X. Nicolas, P. Traoré, A. Mojtabi and J.P. Caltagirone, 'Augmented Lagrangian method and open boundary conditions in 2D simulation of Poiseuille–Bénard channel flow', *Int. J. Numer. Methods Fluids*, **24**, 1–19 (1997).
17. R. Peyret and T. Taylor, 'Computational methods for fluid flow', in *Springer Series in Computational Physics*, Springer, Berlin, 1990.
18. H.A. Van Der Vorst, 'BiCGSTAB: a fast and smoothly converging variant of BiCG for the solution of non-symmetric linear systems', *SIAM J. Sci. Stat. Comput.*, **13**, 631–644 (1992).
19. I. Gustafsson, 'On first- and second-order symmetric factorisation methods for the solution of elliptic difference equations', Chalmers University of Technology, 1978.
20. P. Lebreton, J.P. Caltagirone and E. Arquis, 'Natural convection in a square cavity with thin porous layers on its vertical walls', *Numer. Heat Transf.*, **113**, 892–898 (1991).
21. M.F. Tomé, B. Duffy and S. McKee, 'A numerical technique for solving unsteady non-Newtonian free surface flows', *J. Non-Newtonian Fluid Mech.*, **62**, 9–34 (1996).
22. J.U. Brackbill, D.B. Kothe and C. Zemach, 'A continuum method for modeling surface tension', *J. Comput. Phys.*, **100**, 335–354 (1992).
23. J.C. Martin and W.J. Moyce, 'An experimental study of the collapse of liquid columns on rigid horizontal plane', *Philos. Trans. Serie A, Math. Phys. Sci.*, **244**, 312–325 (1952).
24. C.-W. Wang and S. Osher, 'Efficient implementation of essentially non-oscillatory shock capturing schemes', *J. Comput. Phys.*, **772**, 439–471 (1988).
25. M. Sussman and P. Smereka, 'Axisymmetric free boundary problems', *J. Fluid Mech.*, **341**, 269–294 (1997).
26. F. Perrel, 'Simulation numérique d'écoulements hypersoniques visqueux en d'eséquilibre chimique', *Thèse Doctorale*, Ecole Nationale Supérieure de l'Aéronautique et de l'Espace, 1991.
27. E.G. Puckett, A.S. Almgren, J.B. Bell, D.L. Marcus and W.J. Ridert, 'A high-order projection method for tracking fluid interfaces in variable density incompressible flows', *J. Comput. Phys.*, **130**, 269–282 (1997).
28. W. Tsai and D.K.P. Yue, 'Computation of non-linear free-surface flows', *Annu. Rev. Fluid. Mech.*, **28**, 249–278 (1996).

